frontiers in Earth Science

ORIGINAL RESEARCH
published: 03 June 2015
doi: 10.3389/feart.2015.00020

Incorporation of iodine into apatite structure: a crystal chemistry approach using Artificial Neural Network

Jianwei Wang *

Department of Geology and Geophysics, Center for Computation and Technology, Louisiana State University, Baton Rouge, LA, USA

Materials with apatite crystal structure have a great potential for incorporating the long-lived radioactive iodine isotope (^{129}I) in the form of iodide (I^-) from nuclear waste streams. Because of its durability and potentially high iodine content, the apatite waste form can reduce iodine release rate and minimize the waste volume. Crystal structure and composition of apatite ($A_5(XO_4)_3Z$) was investigated for iodide incorporation into the channel of the structure using Artificial Neural Network. A total of 86 experimentally determined apatite crystal structures of different compositions were compiled from literature, and 44 of them were used to train the networks and 42 were used to test the performance of the trained networks. The results show that the performances of the networks are satisfactory for predictions of unit cell parameters *a* and *c* and channel size of the structure. The trained and tested networks were then used to predict unknown compositions of apatite that incorporates iodide. With a crystal chemistry consideration, chemical compositions that lead to matching the size of the structural channel to the size of iodide were then predicted to be able to incorporate iodide in the structural channel. The calculations suggest that combinations of A site cations of Ag^+, K^+, Sr^{2+}, Pb^{2+}, Ba^{2+}, and Cs^+, and X site cations, mostly formed tetrahedron, of Mn^{5+}, As^{5+}, Cr^{5+}, V^{5+}, Mo^{5+}, Si^{4+}, Ge^{4+}, and Re^{7+} are possible apatite compositions that are able to incorporate iodide. The charge balance of different apatite compositions can be achieved by multiple substitutions at a single site or coupled substitutions at both A and X sites. The results give important clues for designing experiments to synthesize new apatite compositions and also provide a fundamental understanding how iodide is incorporated in the apatite structure. This understanding can provide important insights for apatite waste forms design by optimizing the chemical composition and synthesis procedure.

Keywords: apatite, iodine, nuclear waste forms, fission products, crystal chemistry, Artificial Neural Network, unit cell parameters, channel size

OPEN ACCESS

Edited by:
Zhicheng Jing, Case Western Reserve University, USA

Reviewed by:
Alexander F. Goncharov, Carnegie Institution of Washington, USA
Geoffrey David Bromiley, The University of Edinburgh, UK

***Correspondence:**
Jianwei Wang, Department of Geology and Geophysics, Louisiana State University, E235 Howe-Russell Building, Baton Rouge, LA 70803, USA
jianwei@lsu.edu

Specialty section:
This article was submitted to Earth and Planetary Materials, a section of the journal Frontiers in Earth Science

Received: *25 February 2015*
Accepted: *08 May 2015*
Published: *03 June 2015*

Citation:
Wang J (2015) Incorporation of iodine into apatite structure: a crystal chemistry approach using Artificial Neural Network. Front. Earth Sci. 3:20. doi: 10.3389/feart.2015.00020

Introduction

Production of nuclear energy generates radioactive nuclear wastes. Depending on the fuel cycle option, novel chemical reprocessing and transmutation strategies can result in complicated waste streams with a number of radionuclides including heavy alkaline and alkaline earth elements,

transition metals, minor actinides, and lanthanides. Among volatile radionuclides, ^{129}I is particular challenging because iodine is highly mobile either in gas form or in its reduced form, with a long a half-life of 1.57×10^7 years. In its reduced oxidation state, i.e., I^-, iodide is highly mobile in the environment because it is stable in a wide range of redox potential and pH conditions, and is weakly bounded to the surfaces of silicate minerals and rocks commonly occurring in the environment. Because of these unique properties, iodine deserves special attention for designing durable waste forms for long-term disposal in a geological setting.

A number of waste forms have been considered for ^{129}I. Silver iodide (AgI), with a melting point of 558°C, density of 5.7 g/cm^3, has a very low solubility in water, with a solubility product constant of 8.52×10^{-17} at standard condition (Lide, 2014), which suggests it could be a good candidate for long-term storage. However, AgI itself is not a waste form, and it must be incorporated and packaged into a dense and mechanically durable solid waste form for long-term disposal. Its relatively high vapor pressure at moderate temperature is an issue that limits the thermal processing temperature (Garino et al., 2011a). Because of its low melting point, the temperatures to reach a vapor pressure of 1, 10, 100 Pa are 594, 686, and 803°C respectively (Lide, 2014). The vapor pressures are considered high in terms of the waste processing at high temperature (often greater than 800°C). In addition, AgI is photosensitive, and the ionic silver in AgI may be reduced to metallic silver upon exposed to light. This photochemical process reduces the stability of AgI and increases the cost and environmental risk during the processing, transport, and disposal. Borosilicate glasses have been the most widely adopted material at industrial scales for the immobilization of nuclear wastes (Donald et al., 1997), but it is not a choice for iodine because high iodine loss at the required processing temperature (Garino et al., 2011a). In order to use a glass waste form for iodine, low temperature sintering glasses, which can be processed below the melting point of AgI, are recommended. There are a number of glass waste forms proposed for iodine in the literature including vanadium and lead oxide glasses (Nishi et al., 1996), low temperature sintering Bi-Si-Zn-oxide glasses (Garino et al., 2011b), Bi-P-Zn-oxide glasses (Yang et al., 2013), AgI and $Ag_4P_2O_7$ glass (Sakuragi et al., 2008), and silver aluminophosphate glasses (Lemesle et al., 2014). In many of those low temperature sintering glasses, AgI is still the phase that contains iodine and the glass functions as a matrix that encapsulates AgI. In addition to glasses, other waste forms for iodine have also been considered, including iodide sodalite (Sheppard et al., 2006; Maddrell et al., 2014), hydrotalcite-like layered bismuth-iodine-oxide (Krumhansl and Nenoff, 2011), organic frameworks (MOFs) materials (Sava et al., 2012), cyclodextrins compounds (Szente et al., 1999), uranyl borates (Wu et al., 2011), and apatites (Audubert et al., 1997; Carpena et al., 2001; Uno et al., 2001; Zhang et al., 2007; Le Gallet et al., 2010; Campayo et al., 2011; Stennett et al., 2011; Redfern et al., 2012; Lu et al., 2013; Yao et al., 2014). Each of above proposed waste forms for iodine has its unique advantages and limitations that in some part depend on the disposal condition. Since conditions and settings of a long-term geological disposal may vary, more than one candidate waste form for iodine would be ideal, which would provide flexibility in choosing the strategy for a disposal of the nuclear waste.

Among ceramic waste forms for iodine, materials with apatite structure have a number of advantageous properties including long-term durability and structural and chemical flexibility. Its long-term durability is demonstrated by stability of natural apatite samples over billions of years in earth's history (Gauthier-Lafaye et al., 1996). Its structural and chemical flexibilities are shown in a wide range of chemical substitutions at both a single and different crystallographic sites, and its adaptability of symmetries other than hexagonal symmetry (White and ZhiLi, 2003; White et al., 2005). These flexibilities offer an opportunity to incorporate multiple radionuclides in a single phase ceramics. Because apatite waste forms are single phase, it is relatively simpler to characterize its durability and to evaluate its performance than a multiphase waste form. In addition, the flexibility of chemical substitutions in apatite may be beneficial for incorporating both radionuclides and their decay products. Because its multiple crystallographic sites can be occupied by elements with different charges, changes associated with the valance and identity of the radioactive elements resulting from radioactive decay of those β emitters, e.g., 137-Cs and 90-Sr, could be potentially offset by a charge transfer between the sites and structural distortions within the same phase. This charge transfer and structural distortion, preferably local within a couple of bond distance, would prevent likely phase transition or decomposition due to radioactive decay without compromising the integrity of the phase. For 129-I, the isotope β decays to 129-Xe. The emitted electron could be captured by a variable valance metal ion in the structure and the 129-Xe could remain in the structure as a defect or diffuse away as a gas molecule. Thus, apatite-structured phases may be tolerant against or has potential to mitigate the aging effect of radionuclides from a process so-called radioparagenesis (Jiang et al., 2009, 2010), a structural and chemical transformation process resulting from radioactive decay of radionuclides in a solid phase.

Natural mineral apatite has a chemical composition of $Ca_5(PO_4)_3(OH, F, Cl)$ (Naray-Szabo, 1930; Pan and Fleet, 2002; White et al., 2005; Pasero et al., 2010). Apatite is also one of few minerals produced and used by biological systems. Hydroxyleapatite is the major mineral component of tooth and bone (Wopenka and Pasteris, 2005). The extended apatite subgroup describes minerals with the same crystal structure as apatite but with different compositions by chemical substitutions. There are a large collection of synthetic materials with apatite structure. In this paper, apatite-structured material, or simply apatite, is used for materials having apatite structure. The general formula for apatite-structured materials is $A_5(XO_4)_3Z$, often with hexagonal $P6_3/m$ symmetry (space group number 176). Apatite could also adapt symmetries of $P6_3$, *P-3*, *P-6*, $P2_1/m$, and $P2_1$ while keeping the same structural topology (White and ZhiLi, 2003). The crystal structure is depicted in **Figure 1**. The A cation occupies two crystallographic sites Ca(I) and Ca(II). The molar ratio Ca(I)/Ca(II) is 2:3. The A cation can be substituted by a number of cations including Na^+, K^+, Cs^+, Mg^{2+}, Ca^{2+}, Ba^{2+}, Sr^{2+}, Cd^{2+}, Pb^{2+}, Fe^{2+}, Fe^{3+}, REE^{3+}, and Ac^{4+} (REE: rare earth elements, Ac: actinides). For $Ca_5(PO_4)_3F$, Ca(I) site has

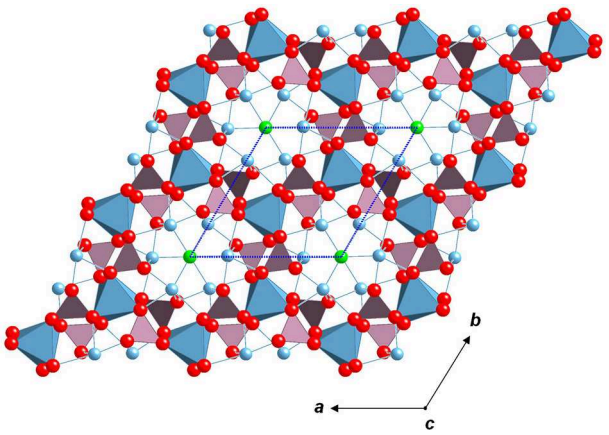

FIGURE 1 | Apatite structure, project on to the (001) plane. The thin dashed blue lines highlight the unit cell. Red ball are oxygen, light blue polyhedrons are Ca(I) cations, the light blue balls are Ca(II) cations, the green balls are channel anions, the purple tetrahedrons are X site cations. The thin light blue lines highlight bonds.

a coordination number of six at Ca(I)-O distance of 2.5 Å and nine at 2.8 Å, and Ca(II) site has a coordination number of six at Ca(I)-O/F distance of 2.5 Å and seven at 2.7 Å (Hughes et al., 1989; White and ZhiLi, 2003). The X cation often forms a tetrahedron with four oxygen atoms and can be substituted by P^{5+}, Si^{4+}, S^{6+}, V^{5+}, Cr^{5+}, As^{5+}, Mn^{5+}, Ge^{4+}. In some cases, the tetrahedron anion group can replaced by non-tetrahedron anions such as ReO_5^{3-} (Baud et al., 1979) and BO_3^{3-} (Campayo et al., 2011). The Z anion in the structural channel can be substituted by OH^-, F^-, Cl^-, Br, I^-, O^{2-}, CO_3^{2-}, and IO_3^-. The chemical substitutions are often coupled between multiple sites. For instance, Ca^{2+} substitution by RE^{3+} at Ca(I)/Ca(II) site is coupled with tetrahedron cation substitution of PO_4^{3-} by SiO_4^{4-} (e.g., $Ca^{2+} + PO_4^{3-} = RE^{3+} + SiO_4^{4-}$). This kind of coupled substitutions involving multiple crystallographic sites is common for apatite and gives apatite-structured materials a unique property that can lead to simultaneous incorporations of multiple radionuclides. For instance, $Sr_8CsNd(PO_4)_6F_{2.3}$, including both Sr and Cs in its structure, was synthesized by a precipitation reaction method (Burakov, 2005). In addition to be used as a host material for storage of nuclear wastes (Audubert et al., 1997; Carpena et al., 2001; Ewing, 2001; Uno et al., 2001; Carpena and Lacout, 2005; Kim et al., 2005; Zhang et al., 2007; Le Gallet et al., 2010; Campayo et al., 2011; Stennett et al., 2011; Redfern et al., 2012; Lu et al., 2013), apatite materials have a number of other applications including bone tissues (Vallet-Regi and Gonzalez-Calbet, 2004), ionic conductors (Arikawa et al., 2000; Kharton et al., 2004), fertilizer (Easterwood et al., 1989), and fission track dating of geological record (Gallagher, 1995; Gallagher et al., 1998). For nuclear waste applications, apatite has be suggested for storage of a number of nuclear wastes including I, Cs, Sr, rare earth elements, and actinides (e.g., U, Th) (Rakovan and Hughes, 2000; Ewing, 2001; Pan and Fleet, 2002; Rakovan et al., 2002; Luo et al., 2009). For iodine incorporation, a lead vanado-iodoapatite $Pb_{10}(VO_4)_6I_2$, a synthetic apatite inspired by a chemically similar natural apatite, lead vanado-chlorapatite (mineral name vanadinite) $Pb_{10}(VO_4)_6Cl_2$, was prepared from $Pb_3(VO_4)_2$ and PbI_2 in stoichiometric amounts using hot-pressing method at a temperature above the melting temperature of PbI_2 (Audubert et al., 1997). Later, lead vanado-iodoapatite was also synthesized by a microwave dielectric heating method using a modified domestic microwave (Stennett et al., 2011). $AgPb_9(VO_4)_6I$ and $AgBa_9(VO_4)_6I$ were synthesized using a solid state reaction method starting with stoichiometric amounts of $Pb_3(VO_4)_2$ and AgI, and $Ba_3(VO_4)_2$ and AgI in a sealed quartz vessels in vacuum and heat-treated at 973 K for 5 h (Uno et al., 2004). Since mineral mimetite ($Pb_5(AsO_4)_3Cl$) has a similar chemical composition as vanadinite, its iodide form, $Pb_5(AsO_4)_3I$, may also be synthesized. Recently, iodate (IO_3^-) was incorporated in hydroxyapaptite structure by precipitation in water (Campayo et al., 2011). High-temperature breakdown of the synthetic $Pb_5(VO_4)_3I$ was characterized and the apatite was observed to be stable until temperature reaches as high as 540°C. A new development of synthesizing iodide-apatite was to combine high energy ball milling and Sparking plasma Sintering (SPS) to synthesize a single phase, almost stoichiometric $Pb_5(VO_4)_3I$ apatite at low temperature with minimum iodine loss (Yao et al., 2014). Excellent radiation resistant and thermal recovery properties were reported for vanadate-phosphate fluorapatite (Lu et al., 2013), silicate-apatite structures (Weber et al., 2012a,b), and actinide-bearing apatites (Weber et al., 1997). A low iodine leach rate of 0.0025 g/m^2/day was reported for synthetic $Pb_5(VO_4)_3I$ apatite at pH 6 and 90°C (Stennett et al., 2011).

As these studies show, apatite has a great potential for storage of a number of radioactive nuclear waste elements because of its long-term durability and irradiation stability. Although materials with apatite structure show excellent properties for various radionuclides, these properties may vary with their chemical compositions. In order to optimize the nuclear waste performance, there is a need to explore the chemical and physical properties and durability of different apatite compositions. However, the chemical substitutions occur at all sites in apatite (i.e., A, X, and Z sites of $A_5(XO_4)_3Z$) and each of these sites can be occupied by a number of elements. The possible apatite compositions could easily reach an unmanageable number only for the end-members. Even for iodide apatite where the iodide is the only Z anion, there are over a hundred possible end-member compositions. It is expected that not all of them are thermodynamically stable and are suitable as waste forms. Experimentally, trying all the combinations would be not only expensive but also time consuming. Thus, it is necessary to be selective by ruling out those that do not meet some basic requirements of the structure and crystal chemistry of apatite. For iodide incorporation in the structural channel, size of the channel in the apatite structure has to fit the size of iodide ion. Currently, only a few iodide apatite compositions have been synthesized experimentally (Audubert et al., 1997; Uno et al., 2004; Campayo et al., 2011; Stennett et al., 2011; Yao et al., 2014). In order to explore other possible compositions, all combinations of elements from the periodic table that meet a basic consideration of the crystal structure and chemical formula should be considered. One of efficient methods to explore a large

number of apatite compositions is Artificial Neural Network (ANN). The method has been previously used to predict the crystallographic cell parameters (Wu et al., 2004; Kockan and Evis, 2010; Kockan et al., 2014) and hardness and fracture toughness (Evis and Arcaklioglu, 2011) of apatite using the average ionic radii of ions at different crystallographic sites. The method has also been used for other crystalline phases (Asadi-Eydivand et al., 2014).

Purpose of this study is to apply Artificial Neural Network method for apatite to predict the size of the structural channel and unknown iodide apatite compositions. By including electron negativity as an additional input parameter in addition to ionic radius, the accuracy of predicted channel size is improved. The simulations provide an understanding of crystal chemistry of apatite and explore unknown apatite with iodide as the channel anion. The results demonstrate that Artificial Neural Network simulation is an effective tool to explore large number of apatite chemical compositions and can be used to predict unknown apatite chemical compositions.

Method—Artificial Neural Networks Simulation

Artificial Neural Network (ANN) approach is inspired from biological neuron assemblies and their way of encoding and solving problems. The philosophy of the approach is to abstract some key ingredients from biology and out of those to construct simple mathematical models. The network consists of an input layer, one or more hidden layers, and an output layer. First, the input data are passed to the input layer with a weight and a bias, and then the results are passed to the neurons in the hidden layers and processed by a training function, and finally the data are passed to the output neuron. There are weighting factors between the neurons of each layer. The predicted output results are compared with actual results, which are used to adjust the weights and biases till the difference between predicted and actual results reaches a predefined criterion (Zhang and Friedrich, 2003). For function approximation, in order to deduce the relationship between the input and the output, a neural network is first trained using a given set of input-output data (typically through supervised learning). After training, such a network can be used as a trained network with an input-output characteristic approximately equal to the relationship of the training problems. Because of the modular and non-linear nature of Artificial Neural Networks, they are considered to be able to approximate any arbitrary function to an arbitrary degree of accuracy, which is particularly useful for non-linear relations. Typically, available data are divided to two subsets, training set and testing set. Validation is needed to calculate the error after each epoch (one cycle of training data). The testing dataset is used to check the ability of the network to predict new data at the end of the training process before the network can be used for predictions (Zhang and Friedrich, 2003; Samarasinghe, 2006; Lucon and Donovan, 2007).

In this study, the available data were divided roughly to half and half, and the training dataset was strategically selected in order to cover the end members of available chemical compositions and some important solid solutions of apatite. A multilayer perception model with supervised learning and batch training was used. A single hidden layer with different numbers of processing units and various learning methods were tested in order to achieve the best network performance and prediction reliability. In the hidden layer, there are a number of commonly used non-linear activation functions. And in this study, hyperbolic tangent sigmoid transfer function was used. The backpropagation algorithm was used. A linear function was used for the output layer. The sigmoid function has a number of advantages for the transfer function in the hidden layer. Its continuity makes it differentiable and minimization of the mean-square error with respect to the weighted sums can be used to adjust the weights of the network during the backpropagation of errors. It has upper and lower bounds, which means even if the inputs are very large, the outputs will never reach large values. Non-linearity makes the functions a natural choice for complex non-linear correlations between inputs and outputs (Samarasinghe, 2006).

The Artificial Neural Network toolbox from Matlab program package was used (The MathWorks, 2011; Demuth and Beale, 2013). A number of training functions have been tried. Levenberg-Marquardt backpropagation is a network training function that updates weight and bias values according to Levenberg-Marquardt optimization. It is often the fastest backpropagation algorithm in the toolbox, and was tested first. Other algorithms tested include resilient backpropagation, BFGS quasi-Newton backpropagation, and Bayesian regulation backpropagation among other algorithms. Using mean-square error with respect to weight and bias as the performance function, the Bayesian regulation backpropagation has the best performance. Bayesian regularization minimizes a linear combination of squared errors and weights. It also modifies the linear combination so that at the end of training, the resulting network has good generalization qualities.

Results and Discussion

Crystallographic Data Set of Apatite-Structured Materials

In order for ANNs to predict properties of unknown apatite of various chemical compositions, a dataset, including chemical composition and crystal structure, of known apatite compositions has to be constructed. The dataset is based on a large number of publications in the open literature and crystal structure databases about apatite. For the iodide incorporation, the channel size is important since the iodide radius is large, 2.2 Å (Shannon, 1976). In order for iodide to be incorporated in the structural channel, the channel size has to be compatible with the size of the ion. Since the coordinates of Ca(II) site in the crystal structure is needed to calculate the channel size, crystal structure information, i.e., chemical composition, occupancies and coordinates of the sites, are needed for the construction of the dataset.

A dataset of 86 apatite compositions was compiled from inorganic crystal structure database (ICSD) and the literature (Wu et al., 2004; ICSD, 2010; Kockan and Evis, 2010), listed in

Supplementary Table 1. The average ion radius is calculated based on the chemical formula and is molar fraction weight-averaged. Because the interaction between the channel anion and Ca(II) site cation in apatite structure is mainly ionic, ionic radii for A and Z ions are used. Ionic radii of all the elements in the periodic table have been compiled in the literature (Shannon, 1976; Henderson, 2000). Ionic radius depends on the coordination number, which in turn is dependent on cutoff bond distance. For apatite, coordination numbers of Ca(I) and Ca(II) sites in $Ca_5(PO_4)_3F$ are 6 at 2.5 Å, or 9 and 7 at 2.8 Å respectively. For this study, two A cation sites are not distinguished. For the consistency between the two sites and across different apatite compositions, coordination number of 6 was used for the ionic radius of A cation when choosing the ionic radius values from the literature. For X site, crystal radius was used, largely because the X cation has a strong covalent bond with oxygen and coordination number is 4 in most of the cases. However, the use of crystal radius should not make difference in ANN simulations because crystal radius differs from ionic radius by a constant of 0.14 Å (Shannon, 1976). The coordination number of the channel Z anion depends on the location of the channel ion, and it is 3 if the ion is positioned in the same (001) plane of the Ca(II) or 6 if in the plane of the Ca(I). Some channel anions can have multiple occupies positioned in a range between the two planes, which are largely dependent on the relative size of the channel anion with respect to the channel size and interactions between the channel anion and Ca(II) cations. For consistency, coordination number of 6 was used for ionic radius parameter of the channel anion. In the previous ANNs studies of apatite (Wu et al., 2004; Kockan and Evis, 2010), ionic radius with a coordination number of 6 was used for the tetrahedron-forming cations, which is not consistent with the structure and coordination of the cations. In the present study, the size of ions was based on the actual coordination and bonding character of the concerned ions, resulting in better overall predictions of the cell parameters. In addition to ionic radius, electronegativity was used as an input parameter because it is important for defining chemical bonding character between the atoms, which in turn affects both the unit cell parameters and channel size. Electronegativity was not used previously in predicting the unit cell parameters (Wu et al., 2004; Kockan and Evis, 2010). We will show in the next section that using electronegativity as an additional input improves the accuracies of the predictions of the channel size and the unit cell parameters. Electron configuration, valence electron, electron localization and delocalization, and electron spin state are all important when considering chemical bonding. However, since these properties are already largely reflected in ionic radius and electronegativity, they are not considered in the present study.

Artificial Neural Network Simulations

The dataset from experimental crystal structure data is divided to two, one for training the networks (i.e., the first 44 apatites in Supplementary Table 1) and one for testing the networks (i.e., the rest, 42 apatites). The training dataset includes the end members of apatite compositions and some of the solid solutions, and the rest of them are included in the testing dataset. This strategy allows the ANNs to be well trained for the predictions of apatite compositions.

Figure 2 illustrates the ANN method used to simulate the cell parameters and channel size of apatite. There are six input parameters, average radius and average electronegativity for each of the three cation sites. There is a hidden layer with four neurons and an output layer. The output has one parameter. The ANN simulations were carried out separately for unit cell parameters *a*, *c*, and channel size.

Using Bayesian regularization (BR) algorithm, the training simulation runs until the algorithm is converged, which is indicated by the convergence of the effective number of simulation parameters, maximum MU (a parameter for controlling convergence algorithms), convergence of the summed square error, and sum squared parameter. For unit cell parameter *a*, the simulation took 130 epochs, and the sum of squared errors (SSE) was converged to 0.0613. The effective number of parameters was found to be 21, and the sum squared parameter was converged to 7.08. These results indicate the BR method successfully minimized the error function and a higher generalization was achieved. Similar results were obtained for unit cell parameter *c* and channel size.

The performance of the ANNs is judged by the errors and the error distributions between predicted and target experimental values. It can be evaluated by the coefficient (i.e., R) of a linear regression between predicted and target experimental values. In contrast to previously studies (Wu et al., 2004; Kockan and Evis, 2010), electronegativity was used as an input in the present study for each of the ions in the ANNs. The results show that, by including the electronegativity, with the same settings of the ANN simulations, the R values are increased by 1.2, 1.3, and 8.8% for the testing set of cell parameters *a*, *c*, and channel size respectively, suggesting that the performance of the ANNs is improved over without using electronegativity as an input parameter. This improvement is especially true for the prediction of the channel size, which is more sensitive to the electronegativity of the atoms.

Prediction of Unit Cell Parameters

For unit cell parameter *a*, the ANN simulation result is shown in **Figure 3** and listed in Supplementary Table 1. The dashed-lines are perfect prediction lines and solid lines are linear regression lines. The fitting coefficient R values of the linear regression

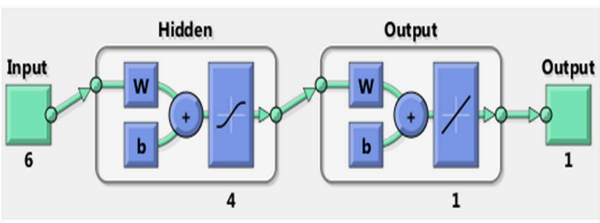

FIGURE 2 | The Artificial Neural Network used for the predictions of apatite compositions and structure parameters. There are six input parameters and one output parameter, one output layer, and one hidden layer. There are 4 neurons used in the hidden layer for the networks.

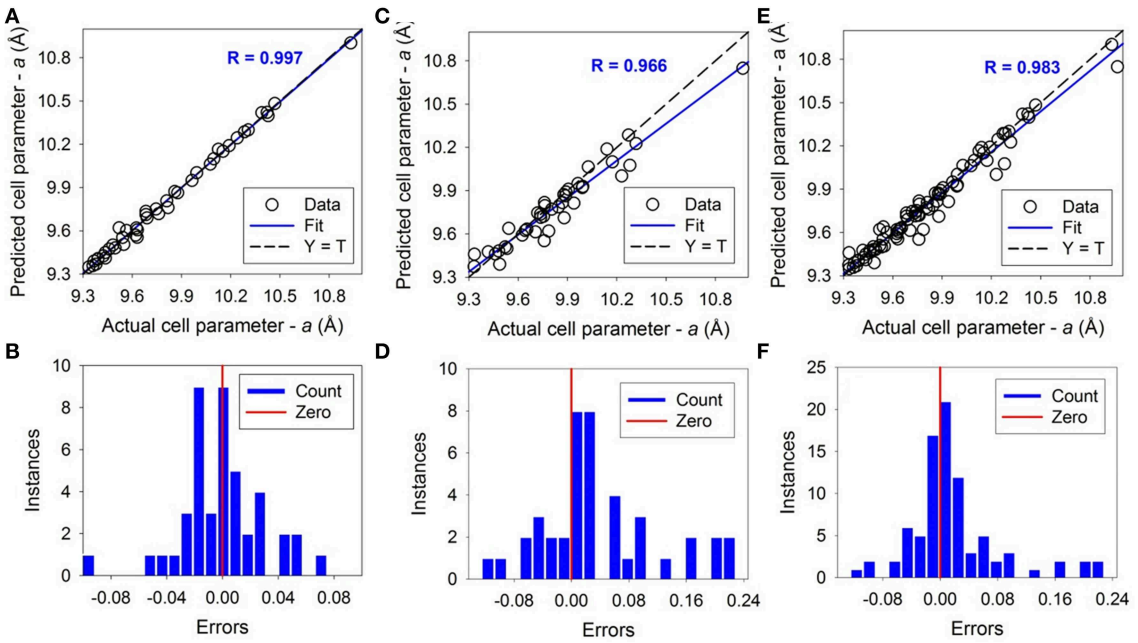

FIGURE 3 | The results of Artificial Neural Network simulations of unit cell parameter *a*. The upper figures show the correlations between predicted and actual values. The bottom figures show the error distributions around the vertical red bars of zero error. The dashed lines correspond to Y = T when the predicted and actual are the same. The solid lines correspond to linear fitting with a fitting coefficient of R. Open circles are experimental data. **(A,B)** are the result of training, **(C,D)** are of testing, and **(E,F)** are of the total.

between the predicted and actual value are 0.997, 0.966, and 0.983 for the training, testing, and overall ANN simulations respectively. The average error between the predicted and actual value is 0.22%, 0.65%, and 0.43% for training, testing and overall dataset respectively. The maximum error is 1.05% for the training dataset and 2.23% for the testing dataset. For unit cell parameter *c*, results are shown in **Figure 4** and also listed in Supplementary Table 1. The coefficient R values are 0.998, 0.977, and 0.989 for the training, testing, and overall ANN simulations respectively. The average errors are 0.20%, 0.67%, and 0.43% for training, testing and overall dataset respectively. The maximum error is 1.35% for the training dataset and 2.29% for the testing. As shown by the error distributions in **Figures 3**, **4**, the errors for the predictions of *a* and *c* are distributed around the averages normally, except a couple of exceptions. These results suggest that the trained and tested ANNs are satisfactory for predicting the apatite cell parameters *a* and *c* of unknown apatite compositions. The results are similar to previous studies using average ionic radii at different sites (i.e., A, X, Z of $A_5(XO_4)_3Z$) to predict the crystallographic unit cell parameters (Wu et al., 2004; Kockan and Evis, 2010).

Figure 5 illustrates how a trained and tested ANN is used for predicting unit cell parameter *a* of unknown apatite compositions with iodide in the channel of the structure. As shown, for any given average radii of A and X site cations, the cell parameter *a* (or *c*) can be predicted by reading into the figure. Since the A and X cations are unknown, their electronegativities have to be assumed (i.e., 2.33 and 1.63 for A and X respectively), which will need to be adjusted for an actual composition. For instance, for A site radius of 1.2 Å and X site radius of 0.4, the predicted *a* cell parameter is ~10.17 Å. For an actual prediction, compositions have to be given and average radii and electronegativities at all sites will need to be calculated and supplied to the trained and tested ANN. This approach is applicable to any apatite compositions with or without iodide in the channel. Giving the flexibility of apatite structure, there is a large number of cations that can occupy A and X cites. Similar figures like **Figure 5** can be generated from ANN simulations to show predictions of the cell parameters as a function of the cation radius.

Although trained and tested ANNs could take any chemical compositions for predicting properties of the apatite, constraints exist as not any combinations of elements at A, X, and Z sites are possible apatite compositions. First, any substitutions at one site or coupled substitutions at multiple sites are constrained by charge balance. For the Z anion, in addition to F, OH, Cl, Br, I, O and vacancy are also possible, and poly-oxyanion are also possible but rare. For the A cation, the valance can deviate from +2 to +1, +3 and +4, indicating a great flexibility of the site incorporating various charged species. For the X cation, in addition to tetrahedral forming cations, cations that can form pyramidal polyhedron like ReO_5^{3-} (Baud et al., 1979) and trigonal pyramidal iodate IO_3^- are also possible in the tetrahedral site (Campayo et al., 2011).

Prediction of Channel Size of Apatite Structure for Iodide Incorporation

For iodide apatite, the channel size of the structure has to be large enough to incorporate iodide ion. For instance, the synthetic

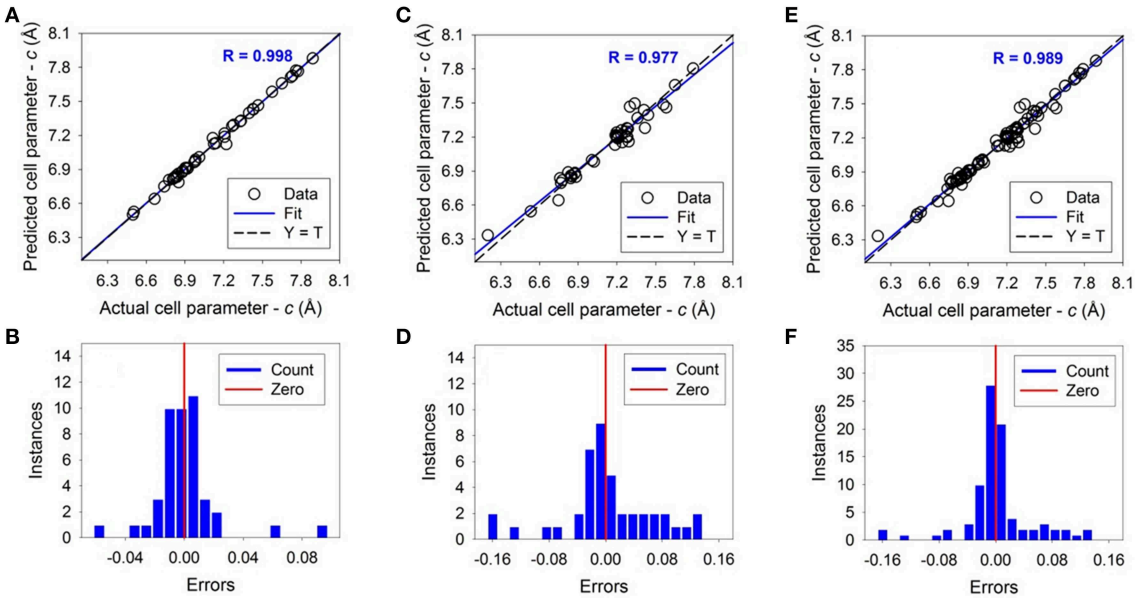

FIGURE 4 | The results of Artificial Neural Network simulations of unit cell parameter *c*. The upper figures show the correlations between predicted and actual values. The bottom figures show the error distributions around the vertical red bars of zero error. The dashed lines correspond to Y = T when the predicted and actual are the same. The solid lines correspond to linear fitting with a fitting coefficient of R. Open circles are experimental data. **(A,B)** are the result of training, **(C,D)** are of testing, and **(E,F)** are of the total.

iodide apatite (i.e., $Pb_5(VO_4)_3I$) has relatively large ion Pb^{2+} in the Ca(I)/Ca(II) sites and VO_4 in the tetrahedron site, leading to a large channel size (Audubert et al., 1997). The success of the synthesis is largely inspired by a natural mineral, vanadinite - $Pb_5(VO_4)_3Cl$, a structurally inflated apatite. The hypothesis is that apatite compositions resulting in the size of the structural channel matching with the size of iodide ion are mostly possible chemical compositions for incorporating iodide. This hypothesis is based on an observation that large channel hosts large anions and small channel hosts small anions. **Figure 6** shows such a correlation between the channel size (predicted and actual) and different anions for a collection of apatites. As shown, the ionic radii of I, Br, Cl, OH, and F are correlated with their respective channel sizes in the apatite structure. If the channel is too small for a given composition, iodide ion would not able to fit in. Thus, the ability to predict the channel size is necessary for predicting unknown iodide apatite compositions.

The ANN simulation for the channel size was carried out similarly to those of the lattice parameters. The channel size is defined as the radius of the largest sphere held in the channel defined by Ca(II) site cations. The training and testing results of the ANN for prediction of channel size are shown in **Figure 7**. As shown, the ANN is well trained with the R values of 0.981, 0.901, and 0.945 for the training, testing and overall respectively. The average errors are 0.75%, 1.45%, and 1.10% for training, testing and overall dataset respectively. The maximum error is 4.10% for the training dataset and 6.29% for the testing. The error distributions are mostly distributed around the averages normally. Although the testing dataset is challenging, extreme outliers are rare. Only two cases are predicted with over 4% off

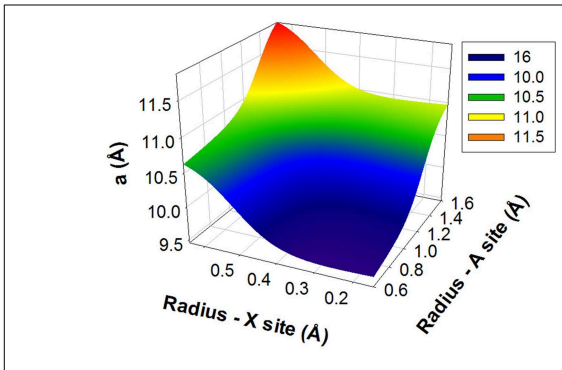

FIGURE 5 | An Artificial Neural Network for the prediction of unit cell parameter *a*. The figure is color coded with red color for high value and blue color for small value. For any given average radii of A and X site cations, the cell parameter *a* can be predicted by just reading the value at the surface of predicted cell parameter *a*.

the experimental values. These results suggest that the trained and tested ANN is satisfactory and can be used to predict the channel size for unknown chemical compositions with iodide in the channel.

To illustrate how to use the trained and tested ANN, **Figure 8** shows a prediction of possible iodide apatite compositions. The optimal radius of the channel should match the combined radius of iodide ion and Ca(II) site cation. For the ionic radius of iodide 2.20 Å and 3.5% flexibility of the structure and error of the ANN prediction, which is set to approximately the maximum error excluding the two extreme cases out of 86 cases, the possible

iodide chemical compositions are those that their X and A site cation average radii fall within the pink curves at X-A plane in **Figure 8**. The corresponding channel size falls at the surface within the pink curves. As it is projected on to the radius-X and radius-A plane, the region between the pink lines is possible average X and A site cations. Thus, possible A site cations include: Ag^{+}, Sr^{2+}, Pb^{2+}, K^{2+}, Ba^{2+}, and Cs^{2+} and possible X site cations include Si^{4+}, Mn^{5+}, As^{5+}, Cr^{5+}, V^{5+}, Re^{7+}, Ge^{4+}, and Mo^{5+}, which are mainly tetrahedron forming cations. Therefore, combinations of A site = Sr^{2+}, Pb^{2+}, Cd^{2+}, Ba^{2+} of 2+ charged cations with ionic radius larger than or close to 1.2 Å, and X site = V^{5+}, As^{5+}, Cr^{5+}, and Mo^{5+} of 5+ charged tetrahedral anion may provide suitable channel size for iodide. In addition, if Si and Ge form the X site tetrahedrons, 3+ charge cations are needed for charge balance at A site. Rare earth cations of the first few elements such as La with ionic radius close or larger

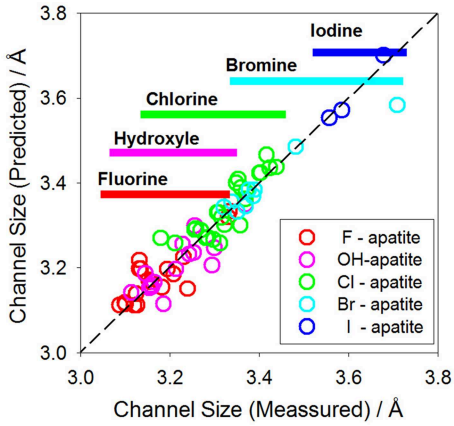

FIGURE 6 | Correlation between the channel size and ionic radius of the channel anion. The open circles are actual experimental data. The horizontal bars correspond to the range of channel size of experimental determined crystal structures. The dashed line corresponds to when predicted and actual values are equal.

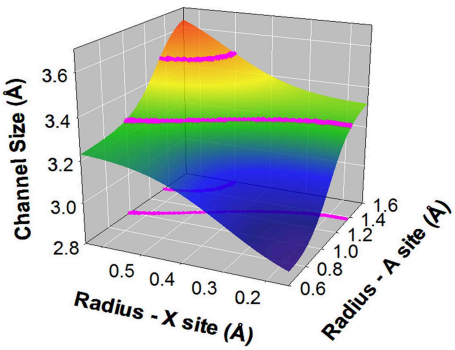

FIGURE 8 | Prediction of unknown apatite compositions with iodide ion in the structural channel. The region between pink lines is possible average radii of A and X cations. The two pink lines define channel size that fits iodide in the structure, which is calculated based on ionic radius of iodide 2.20 Å and 3.5% error prediction. The region is also both projected on to the radius –A and radius-X plane and on to the surface of predicted channel size.

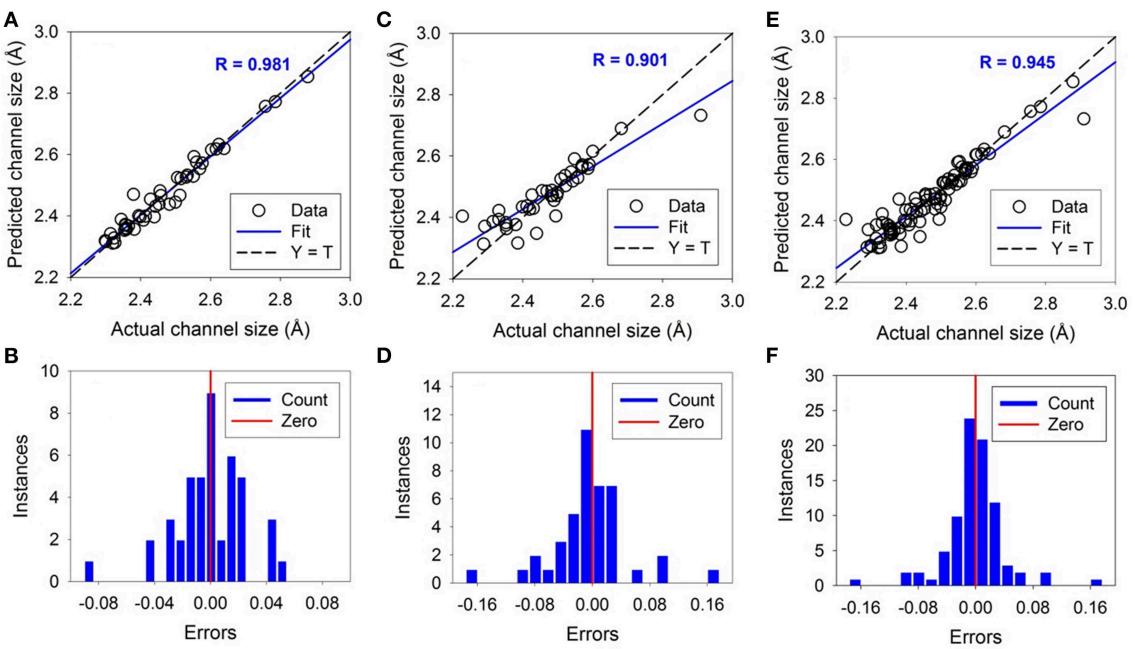

FIGURE 7 | The results of Artificial Neural Network simulations of the channel size. The upper figures show the correlations between predicted and actual values. The bottom figures show the error distributions around the vertical red bars of zero error. The dashed lines correspond to Y = T when the predicted and actual are the same. The solid lines correspond to linear fitting with a fitting coefficient of R. Open circles are experimental data. **(A,B)** are the result of training, **(C,D)** are of testing, and **(E,F)** are of the total.

than 1.2 Å are considered. It is also possible that 1+ charged cations such as Ag^+, Cs^+, K^+ at A site should be able to be incorporated in the apatite structure by coupled substitutions in one or more sites with higher charged ions. Indeed, Ag-Pb-V-I apatite was synthesized using a solid state reaction method (Uno et al., 2004) with the topology of the apatite structure but with a monoclinic symmetry, which is not unusual for apatite group materials (White and ZhiLi, 2003).

Concluding Remarks

Artificial Neural Network simulations of apatite show that the unit cell parameters and the detail of crystal structure (i.e., channel size) can be predicted from its chemical compositions. The results lead to a prediction of a number of possible apatite compositions with iodide incorporated in the structure. Although it is yet to see the accuracy of the prediction, the results provide important clues for designing experiments to synthesize new apatite compositions. It needs to be mentioned that the Artificial Neural Network simulations only consider crystallographic information and doesn't explicitly predict thermodynamics stability of the predicted compositions. The purpose of the simulations is to narrow down potential apatite chemical compositions from over hundreds of possibilities. These small groups of compositions are expected to be manageable by experiments. In order to further narrow down the list using a computational approach, thermodynamic stability of the predicted chemical compositions will need to be estimated by, for instance, first-principles thermodynamics calculations.

The ability to predict the properties of apatite structure using Artificial Neural Network is originated from the fact that there is a strong correlation, although non-linear, between the structure and chemical composition of apatite. In addition, a large structural and compositional database of apatite allows adequate training and testing of the Artificial Neural Networks before predictions can be made. The availability of a large database stems from the facts that there is a wide range of applications of apatite structured materials, and structural and compositional flexibilities of apatite structure, which are demonstrated from the fact that the apatite structure can even be deviated from hexagonal symmetry while maintaining the topology of apatite structure. However, such flexibilities, both structural and compositional, are not unique to apatite structure. Many natural minerals with potential interests to nuclear waste forms have structural and compositional flexibilities similar to apatite, such as powellite related minerals—scheelite and fergusonite ABO_4 (A = Ca, Pb, Ba, Y, La, Ce, Nd, B = Mo, W, Nb, Ti), hollandite AB_8O_{16} (A = Cs, Sr, Ba, Rb, B = Al, Ti, Fe, Mn), crichtonite (Ca, Sr, La, Ce, Y) $(Ti, Fe, Mn)_{21}O_{38}$, murataite $(Y, Na)_6(Zn, Fe)_5(Ti, Nb)_{12}O_{29}(O, F)_{14}$, to name a few. It is expected that the approach of using Artificial Neural Network to predict possible compositions of apatite of incorporating iodide could also be useful for the understanding of the relationship between chemical composition and crystal structure of other crystalline phases including those aforementioned for incorporating various fission products. For non-crystalline materials such as glass nuclear waste form, the structure is often defined at short and intermediate ranges. The local structure surrounding incorporated radionuclides is expected to vary with the composition of the glass as well as the waste composition and level of waste loading. Such variations of the local structure, mostly defined by coordination, bond distances and angles of the glass structural units, suggest structural flexibility of the glasses. The relationship between the structure and incorporated radionuclides in the glasses could then be modeled using similar approaches like Artificial Neural Network as for crystalline phases. This kind of modeling, although often challenging for glasses, is practical for crystalline phases and is imperative to the understanding of the composition-structure-property relation. The results could provide important insights for nuclear waste forms design by optimizing the chemical composition and properties for optimal performance for various nuclear waste elements.

Acknowledgments

This research is being performed using funding received from the DOE Office of Nuclear Energy's Nuclear Energy University Programs under award DE-AC07-05ID14517.

Supplementary Material

The Supplementary Material for this article can be found online at: http://journal.frontiersin.org/article/10.3389/feart.2015.00020/abstract

References

Arikawa, H., Nishiguchi, H., Ishihara, T., and Takita, Y. (2000). Oxide ion conductivity in Sr-doped $La_{10}Ge_6O_{27}$ apatite oxide. *Solid State Ionics* 136, 31–37. doi: 10.1016/S0167-2738(00)00386-6

Asadi-Eydivand, M., Solati-Hashjin, M., Farzadi, A., and Osman, N. A. A. (2014). Artificial neural network approach to estimate the composition of chemically synthesized biphasic calcium phosphate powders. *Ceramics Int.* 40, 12439–12448. doi: 10.1016/j.ceramint.2014.04.095

Audubert, F., Carpena, J., Lacout, J. L., and Tetard, F. (1997). Elaboration of an iodine-bearing apatite Iodine diffusion into a $Pb_3(VO_4)_2$ matrix. *Solid State Ionics* 95, 113–119. doi: 10.1016/S0167-2738(96)00570-X

Baud, G., Besse, J. P., Sueur, G., and Chevalier, R. (1979). Structure de nouvelles apatites au rhenium contenant des anions volumineux: $Ba_{10}(ReO_5)_6X_2$ (X = Br, I). *Mater. Res. Bull.* 14, 675–682. doi: 10.1016/0025-5408(79)90051-5

Burakov, B. E. (2005). *Development of Fluorapatite as a Waste Form: Final Report*. Las Vegas, NV: University of Nevada.

Campayo, L., Grandjean, A., Coulon, A., Delorme, R., Vantelon, D., and Laurencin, D. (2011). Incorporation of iodates into hydroxyapatites: a new approach for the confinement of radioactive iodine. *J. Mater. Chem.* 21, 17609–17611. doi: 10.1039/c1jm14157k

Carpena, J., Donazzon, B., Ceraulo, E., and Prene, S. (2001). Composite apatitic cement as material to retain cesium and iodine. *Comptes Rendus De L Academie Des Sciences Serie Ii Fascicule C-Chimie*, 4, 301–308. doi: 10.1016/S1387-1609(01)01229-4

Carpena, J., and Lacout, J. L. (2005). Calcium phosphate nuclear materials: apatitic ceramics for separated wastes. *Actual. Chim*. 37, 66–71.

Demuth, H., and Beale, M. (2013). *Neural Network Toolbox for use with MATLAB, User's Guide.* Massachusetts: The MathWorks, Inc.

Donald, I. W., Metcalfe, B. L., and Taylor, R. N. J. (1997). The immobilization wastes using ceramics and glasses. *J. Mater. Sci*. 32, 5851–5887. doi: 10.1023/A:1018646507438

Easterwood, G. W., Sartain, J. B., and Street, J. J. (1989). Fertilizer effectiveness of three carbonate apatites on an acid ultisol. *Commun. Soil Sci. Plant Anal.* 20, 789–800. doi: 10.1080/00103628909368117

Evis, Z., and Arcaklioglu, E. (2011). Artificial neural network investigation of hardness and fracture toughness of hydroxylapatite. *Ceramics Int*. 37, 1147–1152. doi: 10.1016/j.ceramint.2010.10.037

Ewing, R. C. (2001). The design and evaluation of nuclear-waste forms: clues from mineralogy. *Can. Miner*. 39, 697–715. doi: 10.2113/gscanmin.39.3.697

Gallagher, K., Brown, R., and Johnson, C. (1998). Fission track analysis and its applications to geological problems. *Annu. Rev. Earth Planet. Sci.* 26, 519–572. doi: 10.1146/annurev.earth.26.1.519

Gallagher, K. (1995). Evolving temperature histories from apatite fission-track data. *Earth Planet. Sci. Lett*. 136, 421–435. doi: 10.1016/0012-821X(95)00197-K

Garino, T. J., Nenoff, T. M., Krumhansl, J. L., and Rademacher, D. (2011a). "Development of iodine waste forms using low-temperature sintering glass," in *Materials Challenges in Alternative and Renewable Energy Vol. 224*, eds G. Wicks, J. Simon, R. Zidan, E. LaraCurzio, T. Adams, J. Zayas, et al. (Westerville, OH: Amer Ceramic Soc.), 305–312.

Garino, T. J., Nenoff, T. M., Krumhansl, J. L., and Rademacher, D. X. (2011b). Low-temperature sintering Bi-Si-Zn-oxide glasses for use in either glass composite materials or core/Shell I-129 waste forms. *J. Am. Ceramic Soc*. 94, 2412–2419. doi: 10.1111/j.1551-2916.2011.04542.x

Gauthier-Lafaye, F., Holliger, P., and Blanc, P. L. (1996). Natural fission reactors in the Franceville basin, Gabon: a review of the conditions and results of a "critical event" in a geologic system. *Geochim. Cosmochim. Acta* 60, 4831–4852. doi: 10.1016/S0016-7037(96)00245-1

Henderson, W. (2000). *Main Group Chemistry*. Hoboken, NJ: Royal Society of Chemistry.

Hughes, J. M., Cameron, M., and Crowley, K. D. (1989). Structural variations in natural F, OH, and Cl apatites. *Am. Mineral*. 74, 870–876.

ICSD. (2010). *Inorganic Crystal Structure Database. Fachinformationszentrum Karlsruhe*. FIZ Karlsruhe: National Institute of Standards and Technology.

Jiang, C., Stanek, C. R., Marks, N. A., Sickafus, K. E., and Uberuaga, B. P. (2009). Predicting from first principles the chemical evolution of crystalline compounds due to radioactive decay: the case of the transformation of CsCl to BaCl. *Phys. Rev. B* 79:132110. doi: 10.1103/PhysRevB.79.132110

Jiang, C., Uberuaga, B. P., Sickafus, K. E., Nortier, F. M., Kitten, J. J., Marks, N. A., et al. (2010). Using "radioparagenesis" to design robust nuclear waste forms. *Energy Environ. Sci.* 3, 130–135. doi: 10.1039/B915493K

Kharton, V. V., Marques, F. M. B., and Atkinson, A. (2004). Transport properties of solid oxide electrolyte ceramics: a brief review. *Solid State Ionics* 174, 135–149. doi: 10.1016/j.ssi.2004.06.015

Kim, J. Y., Dong, Z. L., and White, T. J. (2005). Model apatite systems for the stabilization of toxic metals: II, cation and metalloid substitutions in chlorapatites. *J. Am. Ceramic Soc*. 88, 1253–1260. doi: 10.1111/j.1551-2916.2005.00136.x

Kockan, U., and Evis, Z. (2010). Prediction of hexagonal lattice parameters of various apatites by artificial neural networks. *J. Appl. Crystallogr.* 43, 769–779. doi: 10.1107/S0021889810018133

Kockan, U., Ozturk, F., and Evis, Z. (2014). Artificial-neural-network prediction of hexagonal lattice parameters for non-stoichiometric apatites. *Mater. Tehnol.* 48, 73–79.

Krumhansl, J. L., and Nenoff, T. M. (2011). Hydrotalcite-like layered bismuth-iodine-oxides as waste forms. *Appl. Geochem*. 26, 57–64. doi: 10.1016/j.apgeochem.2010.11.003

Le Gallet, S., Campayo, L., Courtois, E., Hoffmann, S., Grin, Y., Bernard, F., et al. (2010). Spark plasma sintering of iodine-bearing apatite. *J. Nucl. Mater*. 400, 251–256. doi: 10.1016/j.jnucmat.2010.03.011

Lemesle, T., Méar, F. O., Campayo, L., Pinet, O., Revel, B., and Montagne, L. (2014). Immobilization of radioactive iodine in silver aluminophosphate glasses. *J. Hazard. Mater*. 264, 117–126. doi: 10.1016/j.jhazmat.2013.11.019

Lide, R. D. (2014). "Fluid properties - Vapor pressure," in *CRC Handbook of Chemistry and Physics, 95th Edn*, ed W. M. Haynes (Boca Raton, FL: CRC Press), 6–66.

Lu, F. Y., Dong, Z. L., Zhang, J. M., White, T., Ewing, R. C., and Lian, J. (2013). Tailoring the radiation tolerance of vanadate-phosphate fluorapatites by chemical composition control. *RSC Adv*. 3, 15178–15184. doi: 10.1039/c3ra42246a

Lucon, P. A., and Donovan, R. P. (2007). An artificial neural network approach to multiphase continua constitutive modeling. *Composites B Eng*. 38, 817–823. doi: 10.1016/j.compositesb.2006.12.008

Luo, Y., Hughes, J. M., Rakovan, J., and Pan, Y. (2009). Site preference of U and Th in Cl, F, and Sr apatites. *Am. Mineral*. 94, 345–351. doi: 10.2138/am.2009.3026

Maddrell, E., Gandy, A., and Stennett, M. (2014). The durability of iodide sodalite. *J. Nucl. Mater*. 449, 168–172. doi: 10.1016/j.jnucmat.2014.03.016

Naray-Szabo, S. (1930). The structure of apatite $Ca_5(PO_4)_3F$. *Z. Kristallographie* 75, 387–398.

Nishi, T., Noshita, K., Naitoh, T., Namekawa, T., Takahashi, K., and Matsuda, M. (1996). Applicability of V_2O_5-P_2O_5 glass system for low-temperature vitrification. *MRS Proc.* 465, 221. doi: 10.1557/PROC-465-221

Pan, Y. M., and Fleet, M. E. (2002). "Compositions of the apatite-group minerals: substitution mechanisms and controlling factors," in *Phosphates: Geochemical, Geobiological, and Materials Importance,* Vol. 48, eds M. J. Kohn, J. Rakovan, and J. M. Hughes (Hoboken, NJ: Wiley-Blackwell), 13–49.

Pasero, M., Kampf, A. R., Ferraris, C., Pekov, I. V., Rakovan, J., and White, T. J. (2010). Nomenclature of the apatite supergroup minerals. *Eur. J. Mineral*. 22, 163–179. doi: 10.1127/0935-1221/2010/0022-2022

Rakovan, J., Reeder, R. J., Elzinga, E. J., Cherniak, D. J., Tait, C. D., and Morris, D. E. (2002). Structural characterization of U(VI) in apatite by X-ray absorption spectroscopy. *Environ. Sci. Technol.* 36, 3114–3117. doi: 10.1021/es015874f

Rakovan, J. F., and Hughes, J. M. (2000). Strontium in the apatite structure: strontian fluorapatite and belovite-(Ce). *Can. Mineral.* 38, 839–845. doi: 10.2113/gscanmin.38.4.839

Redfern, S. A. T., Smith, S. E., and Maddrell, E. R. (2012). High-temperature breakdown of the synthetic iodine analogue of vanadinite, $Pb_5(VO4)_3I$: an apatite-related compound for iodine radioisotope immobilization? *Mineral. Mag.* 76, 997–1003. doi: 10.1180/minmag.2012.076.4.15

Sakuragi, T., Nishimura, T., Nasu, Y., Asano, H., Hoshino, K., and Iino, K. (2008). Immobilization of radioactive iodine using AgI vitrification technique for the TRU wastes disposal: evaluation of leaching and surface properties. *MRS Proc*. 1107:279. doi: 10.1557/PROC-1107-279

Samarasinghe, S. (2006). *From Data to Models. Neural Networks for Applied Sciences and Engineering*. Boca Raton, FL: Auerbach Publications.

Sava, D. F., Garino, T. J., and Nenoff, T. M. (2012). Iodine confinement into Metal-Organic Frameworks (MOFs): low-temperature sintering glasses to form novel Glass Composite Material (GCM) alternative waste forms. *Ind. Eng. Chem. Res.* 51, 614–620. doi: 10.1021/ie200248g

Shannon, R. (1976). Revised effective ionic radii and systematic studies of interatomic distances in halides and chalcogenides. *Acta Crystallogr. Sect. A* 32, 751–767. doi: 10.1107/S0567739476001551

Sheppard, G. P., Hriljac, J. A., Maddrell, E. R., and Hyatt, N. C. (2006). Silver Zeolites: iodide Occlusion and conversion to Sodalite—a potential 129I waste form? *MRS Proc*. 932, 7. doi: 10.1557/PROC-932-36.1

Stennett, M. C., Pinnock, I. J., and Hyatt, N. C. (2011). Rapid synthesis of $Pb_5(VO_4)_3I$, for the immobilisation of iodine radioisotopes, by microwave dielectric heating. *J. Nucl. Mater*. 414, 352–359. doi: 10.1016/j.jnucmat.2011.04.041

Szente, L., Fenyvesi, E., and Szejtli, J. (1999). Entrapment of iodine with cyclodextrins: potential application of cyclodextrins in nuclear waste management. *Environ. Sci. Technol.* 33, 4495–4498. doi: 10.1021/es981287r

The MathWorks, I. (2011). *MATLAB and Artificial Neural Network Toolbox Release 2011a*. Massachusetts: The MathWorks, Inc.

Uno, M., Kosuga, A., Masuo, S., Imamura, M., and Yamanaka, S. (2004). Thermal and mechanical properties of $AgPb_9(VO_4)_6I$ and $AgBa_9(VO_4)_6I$. *J. Alloys Comp.* 384, 300–302. doi: 10.1016/j.jallcom.2004.04.094

Uno, M., Shinohara, M., Kurosaki, K., and Yamanaka, S. (2001). Some properties of a lead vanado-iodoapatite $Pb_{10}(VO_4)_6I_2$. *J. Nucl. Mater*. 294, 119–122. doi: 10.1016/S0022-3115(01)00462-7

Vallet-Regi, M., and Gonzalez-Calbet, J. M. (2004). Calcium phosphates as substitution of bone tissues. *Prog. Solid State Chem*. 32, 1–31. doi: 10.1016/j.progsolidstchem.2004.07.001

Weber, W. J., Ewing, R. C., and Meldrum, A. (1997). The kinetics of alpha-decay-induced amorphization in zircon and apatite containing weapons-grade plutonium or other actinides. *J. Nucl. Mater*. 50, 147–155. doi: 10.1016/S0022-3115(97)00271-7

Weber, W. J., Zhang, Y. W., and Wang, L. M. (2012a). Review of dynamic recovery effects on ion irradiation damage in ionic-covalent materials. *Nucl. Instrum. Methods Phys. Res. Sect. B Beam Interac. Mater. Atoms* 277, 1–5. doi: 10.1016/j.nimb.2011.12.043

Weber, W. J., Zhang, Y. W., Xiao, H. Y., and Wang, L. M. (2012b). Dynamic recovery in silicate-apatite structures under irradiation and implications for long-term immobilization of actinides. *RSC Adv*. 2, 595–604. doi: 10.1039/C1RA00870F

White, T., Ferraris, C., Kim, J., and Madhavi, S. (2005). "Apatite—an adaptive framework structure," in *Micro- and Mesoporous Mineral Phases,* Reviews in Mineralogy & Geochemistry, Vol. 57, eds G. Ferraris and S. Merlino (Chantilly, VA: Mineralogical Society of America), 307–401.

White, T. J., and ZhiLi, D. (2003). Structural derivation and crystal chemistry of apatites. *Acta Crystallogr. Sect. B*, 59, 1–16. doi: 10.1107/S0108768102019894

Wopenka, B., and Pasteris, J. D. (2005). A mineralogical perspective on the apatite in bone. *Mater. Sci. Eng. C Biomimetic Supramol. Syst*. 25, 131–143. doi: 10.1016/j.msec.2005.01.008

Wu, P., Zeng, Y. Z., and Wang, C. M. (2004). Prediction of apatite lattice constants from their constituent elemental radii and artificial intelligence methods. *Biomaterials* 25, 1123–1130. doi: 10.1016/S0142-9612(03)00617-3

Wu, S., Wang, S., Simonetti, A., Chen, F., and Albrecht-Schmitt, T. E. (2011). Incorporation of iodate into uranyl borates and its implication for the immobilization of I-129 in nuclear waste repositories. *Radiochim. Acta* 99, 573–579. doi: 10.1524/ract.2011.1864

Yang, J. H., Shin, J. M., Park, J. J., and Park, G. (2013). Waste form of silver iodide (AgI) with low-temperature sintering glasses. *Sep. Sci. Technol.* 49, 298–304. doi: 10.1080/01496395.2013.817424

Yao, T., Lu, F., Sun, H., Wang, J., Ewing, R. C., and Lian, J. (2014). Bulk iodoapatite ceramic densified by spark plasma sintering with exceptional thermal stability. *J. Am. Ceramic Soc*. 97, 2409–2412. doi: 10.1111/jace.13101

Zhang, M., Maddrell, E. R., Abraitis, P. K., and Salje, E. K. H. (2007). Impact of leach on lead vanado-iodoapatite $Pb_5(VO_4)_3I$: an infrared and Raman spectroscopic study. *Mater. Sci. Eng. B Solid State Mater. Adv. Technol*. 137, 149–155. doi: 10.1016/j.mseb.2006.11.003

Zhang, Z., and Friedrich, K. (2003). Artificial neural networks applied to polymer composites: a review. *Composites Sci. Technol.* 63, 2029–2044. doi: 10.1016/S0266-3538(03)00106-4

Conflict of Interest Statement: The author declares that the research was conducted in the absence of any commercial or financial relationships that could be construed as a potential conflict of interest.